Two-dimensional dynamics of divertor detachment at ASDEX Upgrade

OPEN ACCESS
IOP Publishing
Plasma Physics and Controlled Fusion
Plasma Phys. Control. Fusion **67** (2025) 075016 (9pp)
https://doi.org/10.1088/1361-6587/ade62e

Two-dimensional dynamics of divertor detachment at ASDEX Upgrade

S Hörmann[1,2,*], M Cavedon[3], M Griener[1], D Wendler[1], D Brida[1], E Wolfrum[1], U Stroth[1] and the ASDEX Upgrade Team[1,4]

[1] Max Planck Institute for Plasma Physics, 85748 Garching, Germany
[2] Technical University of Munich, TUM School of Natural Sciences, Physics Department, 85747 Garching, Germany
[3] Dipartimento di Fisica G. Occhialini, Universitá di Milano-Bicocca, Milano, Italy

E-mail: sebastian.hoermann@ipp.mpg.de

Received 7 May 2025, revised 13 June 2025
Accepted for publication 19 June 2025
Published 27 June 2025

Abstract

A newly installed thermal helium beam diagnostic in the outer divertor of ASDEX Upgrade (Hörmann *et al* 2024 *Rev. Sci. Instrum.* **95** 113507) was used for the first time to analyse two-dimensional (2D) electron temperature, density and pressure profiles. This diagnostic measures profiles with unprecedented spatial and temporal resolution, enabling the analysis of detachment transitions from onset state to fluctuating state in L-mode, including smooth transitions, detachment cliffs, and self-sustained divertor oscillations (SSDOs). This is a novelty for detachment studies, as such high-resolution 2D measurements have been lacking up to now, especially during the transitions between different divertor states. We focus on the pressure conservation and the behaviour of n_e and T_e along and perpendicular to the flux surfaces in the different phases of the transition. In addition, the propagation direction and velocity of the temperature collapse during SSDOs are investigated for the first time. They travel in the direction from the near scrape-off layer towards the far scrape-off layer and from the target towards the X-point at a velocity of a few tens of meters per second in the poloidal plane. This measurement is compared with the current models of SSDOs and detachment cliff generation.

Keywords: divertor, detachment, 2D profiles, helium beam, self-sustained divertor oscillations, detachment cliff

1. Introduction

One of the most important topics for large-scale fusion devices like ITER or DEMO is the exhaust problem [1, 2]. This refers to the fact that in, for example ITER, the peak heat fluxes to the divertor can rise up to 40 MW m^{-2} [1]. However, current divertor concepts like the monoblock design for ITER are only designed for stationary power loads up to 10 MW m^{-2} which can go to 20 MW m^{-2} for short time [3, 4]. To overcome this problem, it will be necessary to have a highly dissipative divertor in which a large part of the incoming energy is dissipated, for example, by strong radiation. A key process to do so is detachment, which describes a phenomenon in which the divertor temperature and the particle and heat flux to the divertor tiles stay low. In ITER, for example, it will be necessary to keep the divertor constantly in at least partial detachment [1]. To ensure this, a detailed understanding of the physics involved in entering into the detachment state is essential.

Detachment is routinely obtained in many tokamaks [5–7]. In general, there are three divertor regimes: attached, partially

[4] See Zohm *et al* 2024 (https://doi.org/10.1088/1741-4326/ad249d) for the ASDEX Upgrade Team.
[*] Author to whom any correspondence should be addressed.

detached and completely detached. In the attached scenario, the heat flux goes directly and unmitigated to the divertor tiles. To prevent this, the density in the divertor can be increased, which causes a drastic drop in the temperature, due to ionisation and radiation losses. With high enough density, the particle and heat flux to the target also decreases, this is called the rollover. If this drop occurs along the entire target and reaches a level where the target particle flux is negligible, it is referred to as a complete detachment, while partial detachment is defined if only the area close to the strike line $\approx 2\lambda_q$ is affected [8]. Potzel *et al* [9] proposed another classification of divertor detachment in L-mode. It divides the transition to detachment into three states: the onset state (OS), when the inner divertor is detached, the fluctuating state (FS), where a radiative oscillating signal around the X-point appears [10], and the complete detachment state. The transition to partial detachment typically happens in the FS. Due to the good measurability of the FS, this paper uses the definition according to [9].

A transition between OS and FS can be either smooth or bifurcated [11]. A distinction is generally also made between two bifurcation processes: the detachment cliff, a single transition from attached to partially detached, and the self-sustained divertor oscillations (SSDOs), in which the state oscillates several times between attached and partially detached [12]. In [13–15], a one-dimensional (1D) theory is developed to explain the SSDO: above a certain total number of ions and neutral particles N_d in a flux tube, the heat flux is no longer sufficient to maintain the plasma recycling flux since all the energy is used for ionisation. This leads to a multi-valued $T_d(N_d)$ dependency, with the divertor temperature T_d being a function of N_d, which allows for bifurcations. Such a process can cause a collapse of the recycling, which leads to a transition into a partial detachment. At ASDEX Upgrade, this oscillation was found by [9]. A deeper investigation indicates, that the oscillation is driven by the interplay of inner and outer divertor plasma [12]. The crucial factors are hence the opacity for neutral particles between the inner and outer divertor and the $\boldsymbol{E} \times \boldsymbol{B}$ drift and thus the ion flux Γ_{ion} from the outer to the inner divertor in favourable configuration.

Also, a single bifurcation process from attached to partial detached can occur [11]. This process was first found in DIII-D [16] and is called detachment cliff. The explanation for this phenomenon is that the $\boldsymbol{E} \times \boldsymbol{B}$ drift in the outer divertor transports enough charged particles to the inner divertor [17, 18]. Due to this, the outer divertor stays at high temperature and low density while the inner divertor detaches. However, since the $\boldsymbol{E} \times \boldsymbol{B}$ drift depends on the divertor temperature, which in turn depends on the $\boldsymbol{E} \times \boldsymbol{B}$ drift due to its particle transport, it is possible that a bifurcation process to detachment can occur. The importance of the $\boldsymbol{E} \times \boldsymbol{B}$ drift for the detachment cliff was also confirmed by SOLPS transport code simulation [19]. Recent studies on ASDEX Upgrade also suggested that SSDOs and the detachment cliff could be the result of the same physical process [11].

This work uses a newly installed thermal helium beam in the outer divertor of ASDEX Upgrade [20] to investigate these transitions, based on two-dimensional (2D) measurements with high spatio-temporal resolution. These measurements follow up the DIII-D [18, 21] and ASDEX Upgrade [22] 2D measurements of different divertor states using the Thomson scattering diagnostic. However, the measurements presented here have the fundamental advantage of not needing any plasma sweep to create a full 2D map. 1D and 2D density and temperature profiles during a smooth and an abrupt detachment are analysed in section 2 and section 3. In section 4, the propagation direction and velocity of the temperature collapse in SSDOs is investigated. The measurement results will be compared with the models of [12–15] about SSDOs and that of [17] about the detachment cliff. The last section 5 summarises the main results.

2. 1D investigation of a smooth transition from OS to FS

To investigate the behaviour of density, temperature, and pressure along a magnetic flux surface during a smooth transition from OS to FS, a 1D analysis is performed. A 2D analysis of the smooth transition was not possible due to the lack of measurement points during the used AUG discharge #41132. The main tool for this analysis is the divertor helium beam (DHB) diagnostic [20], which has a similar setup as the helium beam diagnostic in the midplane [23]. The advantages of the DHB are its high spatial (see figure 1) and temporal resolution (1.1 µs), which is achieved by using a polychromator with 32-channel photomultiplier tube arrays [23]. Figure 1 shows a schematic of the DHB. Here, the blue lines mark the helium cloud injected via an in-vessel piezo valve [24], while the measurement points with their resolution are marked with green. For the 1D analysis, the second row of channels counted from the left was used (see figure 1 red marked points). To determine the electron density and temperature a static model [20] is utilised.

The AUG discharge #41132 studied here is an unseeded L-mode with only ohmic heating, a plasma current of 0.79 MA and a toroidal B-field of 2.90 T. The discharge features a slow density ramp, as shown in figure 2(a), with a deuterium fueling rate ranging from 0.1×10^{22} to 0.8×10^{22} atoms s^{-1}. As a consequence of the comparably low heating power, we do not see a bifurcation but a slow, smooth transition to the FS in density and temperature [11]. This can be seen from the signal of the Langmuir probes (LPs) in figure 2(b). The X-point fluctuations of about 6 kHz that define the FS [9, 10] start to appear at 2.127 s, as can be seen in the spectrogram of a bolometer channel observing the X-point in figure 2(c).

Figures 2(d)–(f) show the results of the analysed DHB signal. The dark grey areas indicate the phase where the passive helium background is measured. In the first puffing phase, the divertor is completely in OS. In this phase, the density and temperature gradients are shallow along the field lines or non-existent in the case of pressure. During the FS, i.e. in the second puffing phase, the temperature in the divertor drops. Along the flux surface, gradients in temperature and density

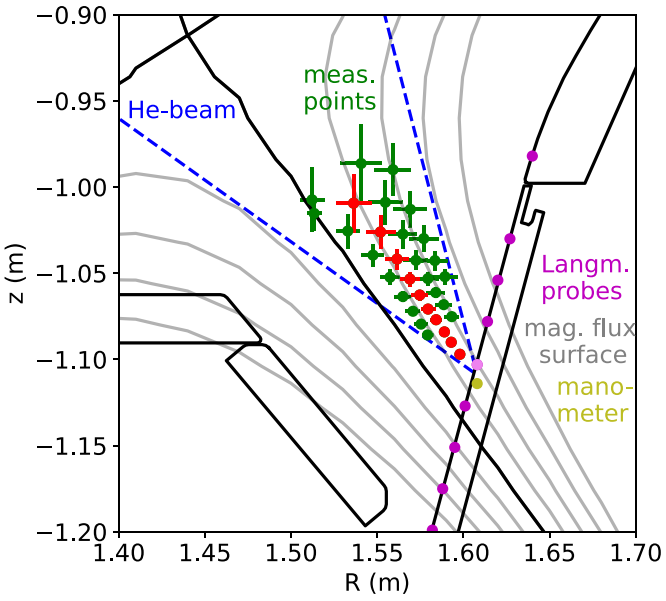

Figure 1. Schematic 2D representation of the DHB. In green, the measurement points, including the spatial resolution, are shown. The dashed blue line shows the position where the helium density drops to $1/e$ of the maximum helium density. The grey lines show the magnetic flux surfaces, with the separatrix in black. The measurement points for figure 2 are marked in red. In purple, the Langmuir probes (LPs) are marked while the LP plotted in figures 2 and 4 is indicated in light violet. The yellow point gives the position of the outer strike-line manometer.

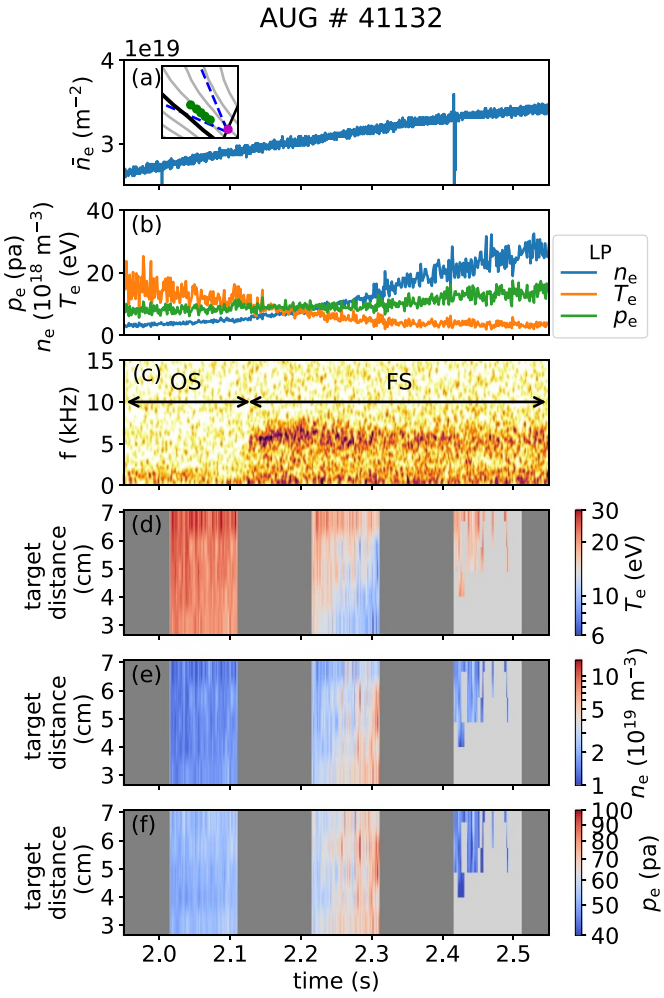

Figure 2. (a) Density ramp of AUG #41132 measured by interferometer. The inlet gives a schematic picture of the divertor region, with its measurement position of the DHB marked in green and the Langmuir probe (LP) in purple. The measured LP density, temperature and pressure signal are plotted in (b). In (c), the spectrogram of a bolometer pointing in the direction of the X-point is plotted. The DHB signals of temperature (d), density (e), and pressure (f) are plotted in the colour code below. The y-axis of the plots indicates the distance along the flux surface to the wall, while the x-axis represents time. The dark grey areas show the parts where no helium was puffed, while the light grey areas represent the time points where no density and temperature reconstruction were possible.

are observed, where the gradient in temperature points towards the X-point and the density gradient in the opposite direction. In addition, the helium beam, like the LPs, shows a temporal decrease in temperature and an increase in density at all five measurement points over the puffing phase. On the other hand, the pressure is constant along the flux surfaces in this phase and increases with time on the way towards detachment. This proves that in this early phase of the FS, the divertor is still in the high recycling regime as described by [9].

The third puffing phase reveals the limitations of the diagnostic. The light grey areas in some channels symbolise time points at which it was not possible to reconstruct the temperature and density. This is because the temperature in this region is too low to have sufficient excited helium. Even in the areas where it was possible to reconstruct, the errors are significantly increased due to the low emission. Nevertheless, qualitative information about the temperature can be obtained from the limit at which the signal breaks off. It starts near the target and goes upwards with time. Therefore, we can see that the temperature near the target is lower than towards the X-point, as well as that the divertor region cools down further.

This measurement gives an entirely new insight into the local dynamic of electron density, temperature and pressure along the flux surfaces during an OS to FS transition. With this, it is possible to show the evolution of an T_e and n_e gradient along the flux surface, as well as proving pressure conservation. The absence of a pressure gradient also proves that the plasma in the outer divertor in the early stages of FS is still attached.

3. 2D measurements of the fast transition from onset to FS

For this 2D electron temperature, density and pressure profile reconstruction during FS and OS, discharge #40015 from AUG was used, an unseeded L-mode. Heated by 0.45 MW of ECRH, it has a toroidal field of 2.90 T and a plasma current of 0.79 MA. Compared to #41132 of section 2, a higher fueling with higher input power was used, see figures 3(a) and (b). The higher heating power leads to a bifurcation from attached to partially detached called detachment cliff [11, 17]. The transition happens at 3.06 s, and leads to an abruptly increasing divertor neutral density n_n and electron density n_e as well as a

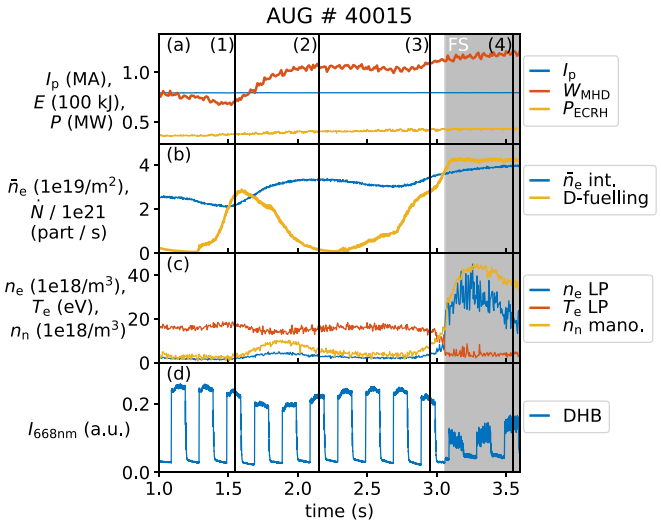

Figure 3. Time traces of the most important divertor quantities for discharge #40015. The figure shows the plasma current (blue), the diamagnetic energy (red) and the ECRH power (yellow) in (a), the line integrated density from the interferometer signal (blue) and the deuterium fueling rate (yellow) in (b). Plot (c) gives the density (blue) and temperature (red) measured by the Langmuir probe and the neutral density measurement the manometer (yellow) at the outer strike-line. The DHB signal of the helium line intensity at 667.8 nm is shown in (d). The black vertical lines indicate the time points of the profiles in figure 4. The grey shaded area marks the fluctuating state (FS).

drop in electron temperature T_e, see figure 3(c). For this discharge, only 24 LOS of the DHB were connected, leaving the channels closest to the X-point unused.

Figure 4 shows the n_e, T_e and p_e profile evaluation at four time points of discharge #40015. For this reconstruction, DHB data are evaluated with a dynamic model, including line integration and dynamic state mixing [20]. The time points are marked in figure 3 by black vertical lines. While in the first two, the divertor is attached, in the third, the divertor is on the verge of a transition to the FS, while in the last one, it is deep in the FS. In all these measurements, the strong decline of n_e, T_e and p_e towards the PFR is visible. In the case of temperature, it is slightly milder than for density. This also applies to the drop in the SOL. The pressure is rather constant along a magnetic flux surface. This confirms pressure conservation along magnetic flux surfaces in the measurement region of the outer divertor for the OS. Only in (i) is a slight pressure gradient near the target visible. There is also a strong indication of pressure conservation in FS, but this cannot be conclusively demonstrated due to the systematic underestimation of density, which is shown in [20]. The source provides a cross-diagnostic comparison involving divertor Thomson scattering. While the two diagnostics agree well on the electron density and electron temperature in OS, and on T_e during FS, the density is underestimated by 30%–50% in FS [20].

At the first two time points in OS, the density and pressure in the divertor slightly increase with the core density while the temperature stays almost the same. Prior to the OS to FS transition, the density increases considerably at 2.95 s, but the temperature decreases only slightly, leading to an increase in pressure. With the transition to the FS, a strong temperature drop appears in the measurement region of the DHB. At the same time, the density rises strongly by a factor of about 3, while the actual rise could be even higher since the DHB underestimates the density in this regime [20]. In the FS, there is a noticeable temperature and density gradient parallel to the flux surfaces, similar to what is observed in section 2. For the pressure, we observe a decline from OS to FS. However, it should be noted that our pressure measurements are underestimated, similar to the density. Therefore, it is not possible to conclusively determine within the uncertainties whether this represents a genuine drop in pressure.

4. Movement of the detachment cliff

To understand the process of the bifurcating transition of divertor states, we now take a deeper look at a SSDO. Here, discharge #40903 of AUG is analysed. As the other two discharges, it is an unseeded L-mode with a plasma current of 0.79 MA and a toroidal B-field of 2.9 T. It is heated by 0.45 MW ECRH. Furthermore it also has a density ramp between 2.5×10^{19} and 6.0×10^{19} m^{-3} caused by a deuterium fueling ramp from 0.2×10^{22} to 2.3×10^{22} atoms s^{-1}. The discharge develops four SSDOs from OS to FS which take place from 2.30 s to 2.51 s. Three of them were measured with the DHB, and the fourth was in a beam-off phase. The signals of the LP and bolometer during this oscillation are shown in figures 5(a) and (c). The characteristic X-point fluctuation at about 6 kHz is visible in the spectrogram of the bolometer signal (b). Also, discharge AUG #40904 was used, which is shown later and identical to #40903, only with slightly higher fueling. In the following the fast transition phase of the oscillation behaviour will be investigated.

For the following analysis with the DHB, the raw intensity signal of the 587 nm and 667 nm lines are investigated, using the full time resolution of 900 kHz. Due to the rapidly changing background during the transition, it was not possible to perform a proper background subtraction. Furthermore, the 706 nm and 728 nm lines have low intensities and, therefore, large uncertainties. For these reasons, density and temperature reconstructions could not be performed. Moreover, because of the missing proper background subtraction, line ratios have to be handled carefully, which is the reason why single line intensities are dominantly used in this section. Only for the proof of concept, the ratios $I_{667\,nm}/I_{728\,nm}$ and $I_{728\,nm}/I_{706\,nm}$ are shown. The measurements are evaluated at five different positions along a magnetic flux surface, and displayed in figure 6. A first observation is, that the transition process and, therefore, the temperature collapse lasts about 2.5 ms (as expected from [11]) and that the temporal offset between the different channels is much smaller than the transition time.

The shape of the signals can be explained by its dependencies

$$\epsilon\left(n_{He}, n_e, T_e\right) = n_e n_{He} \mathrm{PEC}\left(n_e, T_e\right) \quad (1)$$

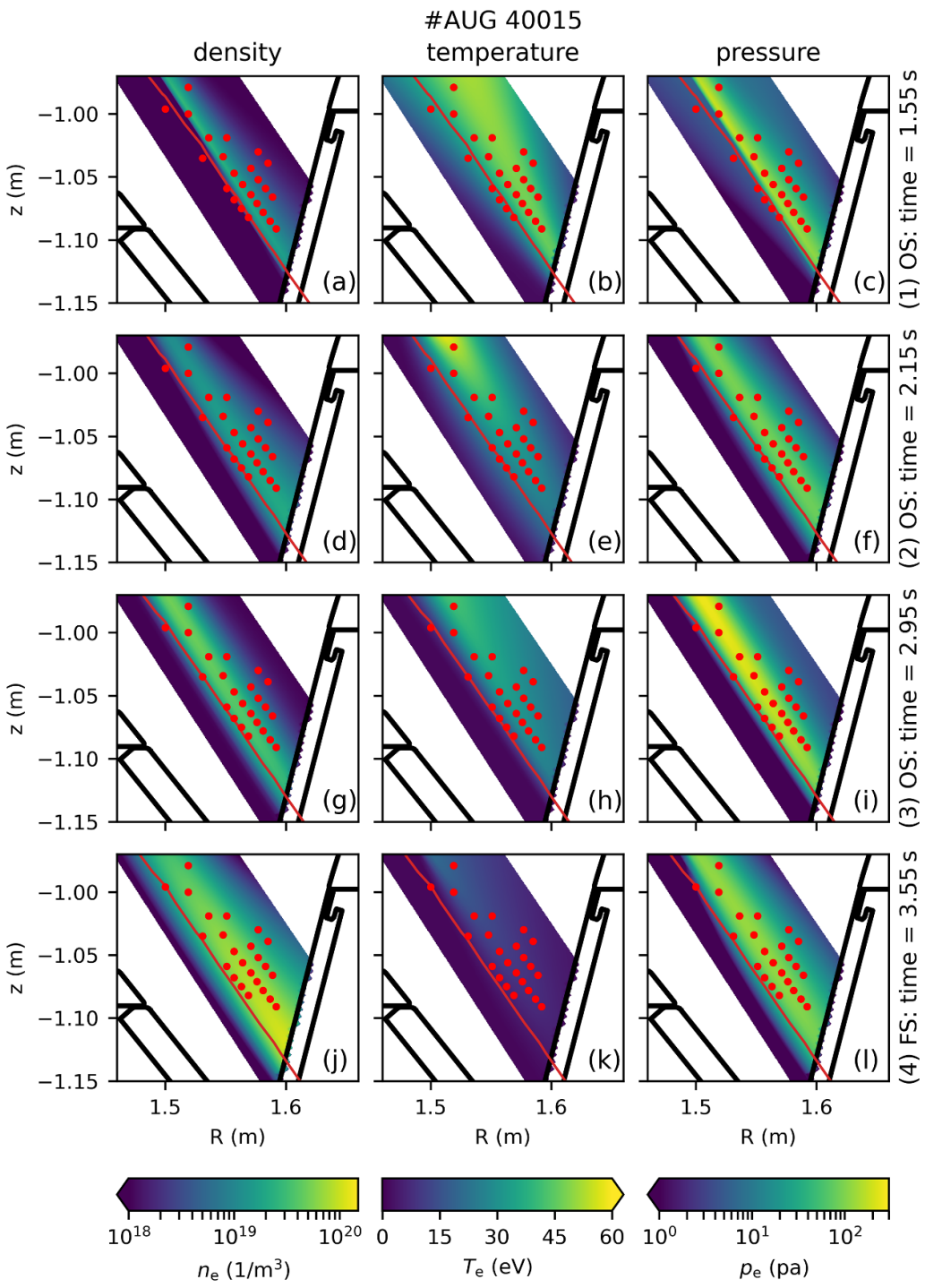

Figure 4. Electron density, temperature, and pressure profiles in the outer divertor of ASDEX Upgrade calculated with a dynamic model by using helium beam data. Four time points with increasing core densities of discharge #40015 are shown. The separatrix and the geometrical measurement points of the helium beam diagnostic are plotted in red.

with ϵ the emission, PEC the photon emissivity coefficient and n_{He} the neutral helium density. For low T_e and high n_e, the electron density has only minor effects on the intensity. This is illustrated in figure 7(a) which shows $n_e \cdot \mathrm{PEC}(n_e, T_e)$. The SSDOs are located at low temperatures and high densities, a region in which the contour lines are almost exclusively vertical and thus show a pure T_e dependence.

The signal shape of figure 6 is made up of four main components: a flat phase in the OS state at the beginning, an elevated signal at the start of the transition followed by a steep drop and a flat phase in the final FS. Due to the temperature collapse in the divertor during a SSDO, the puffed helium is less ionised. This leads to an increase in neutral helium density and, therefore, an enhanced signal. At the same time, the temper-

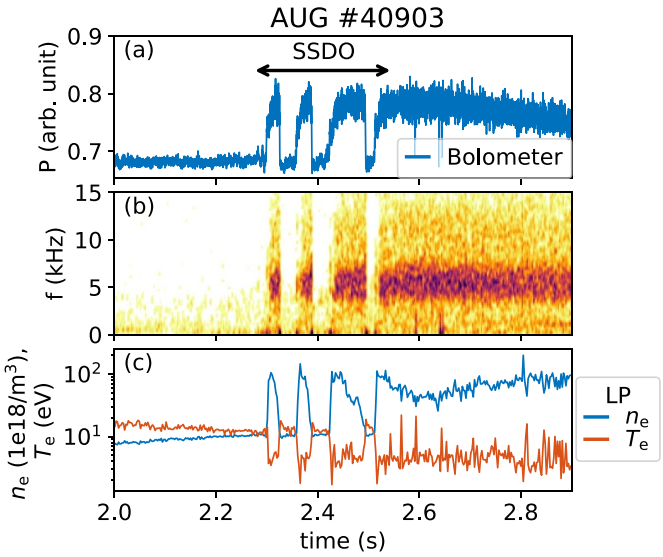

Figure 5. Bolometer (a) and LP (c) signal during the SSDOs of AUG discharge #40903. In (b), the spectrogram of the bolometer signal is plotted with the X-point fluctuation at about 6 kHz.

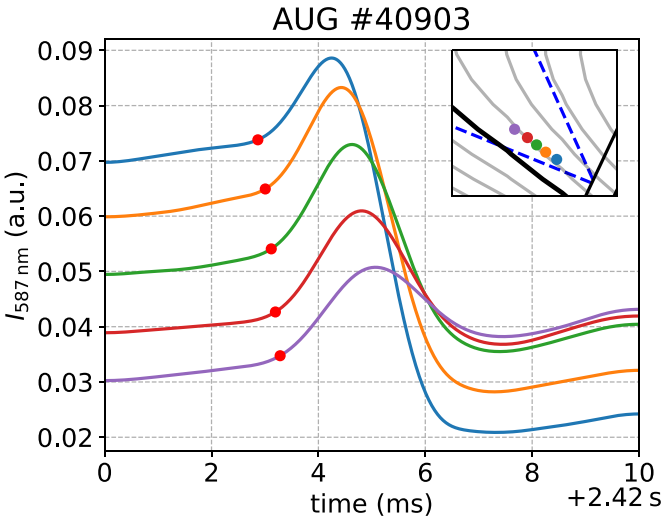

Figure 6. Intensity at 587 nm of five DHB LOS on a magnetic flux surface for the transition from OS to FS. The position of the LOS is marked in the inlet. The red dots describe the maximum curvature point at the beginning of the transition. All curves are smoothed with a sliding Hanning window of length 2.5 ms.

ature drop itself leads to a reduction of the signal, as shown in figure 7(a). Therefore, the signal increases at first, since the neutral helium initially exceeds the lower excitation rate of the falling temperature. In the later phase, this ratio changes, leading to a steep drop. This can be confirmed by the fact that line ratios do not show the described peak, see figure 7(b). As line ratios do not depend on the helium density, see equation (1), the peak arises as a result of the influence of neutral helium particles.

Thanks to the high spatial resolution of the diagnostic, we can investigate how this transition evolves perpendicular to the target plate. For this, the time offsets between the signals of five channels along a magnetic flux surface are investigated. To accomplish this, two methods are employed. The first one uses the maximum of the curvature at the start of the transition as a characteristic point. This point is marked with red in figure 6. It should be noted that for this determination, the signal must be strongly smoothed in time for each channel with a sliding Hanning window of 2.5 ms. The resulting reconstructed propagation starts at the target and propagates upwards with a velocity of $(65 \pm 40)\,\mathrm{m\,s^{-1}}$. The statistical uncertainty was determined via the measurements of two different emission lines, during three OS to FS transitions, as well as the systematic uncertainty via the inaccuracy of the measurement position. Furthermore, by using the same analysis for different smoothing window sizes, the influence of the smoothing was estimated, and the standard deviation between the results was added to the systematic uncertainty.

For the second method, the temporal shift of neighbouring channels is determined by minimising the area between the two curves. This method of determining the time shift is applicable when the signals of neighbouring channels are similar in shape. This is the case for neighbouring parallel channels, see figures 6 and 8, as well as for neighbouring perpendicular channels (not shown here). The procedure for determining the temporal shift is shown in figure 8 where, for illustration purposes, a sliding Hanning window of 1.0 ms is used to smooth the individual signals. The signals were normalised by their lowest and highest values to compensate for the different absolute intensities. The original measured signals are shown in (a), where green marks the area between the two curves that is to be minimised. In (b), the orange curve is shifted by 147 µs for which the area is minimal. For this method, only neighbouring channels are compared as the signals depend on the background density and temperature and are, hence, most similar for neighbouring channels. With this information, the cumulative temporal shift is calculated for each channel and plotted against the distance between the channels to determine the velocity via a linear fit, see figure 9. The uncertainty of the measurement position gives the distance uncertainty, while for the time shift between the channels, the statistic uncertainty determined from the slightly different results between the two wavelength and three transitions is used. For the combined analysis of three transitions and two wavelengths, a smoothing of 10 µs is used. The resulting propagation of the detachment cliff starts at the target and propagates upwards along the flux surface with a constant velocity of $(58 \pm 10)\,\mathrm{m\,s^{-1}}$ in the measurement range between 3 and 7 cm away from the target. The same method was also used for a measurement perpendicular to the magnetic flux surfaces. This results in a velocity of $(41 \pm 12)\,\mathrm{m\,s^{-1}}$ starting from the separatrix in the direction of far SOL. This result should be treated with caution, as only three measuring points were available in this direction. Since the injection velocity of neutral helium is $(1870 \pm 270)\,\mathrm{m\,s^{-1}}$ [26], the determined velocities, which are in the order of $10\,\mathrm{m\,s^{-1}}$, cannot be explained with the helium propagation. Discharge #40904, in which also three SSDOs were measured, shows the same parallel $(63 \pm 10)\,\mathrm{m\,s^{-1}}$ and perpendicular $(48 \pm 9)\,\mathrm{m\,s^{-1}}$ propagation velocity.

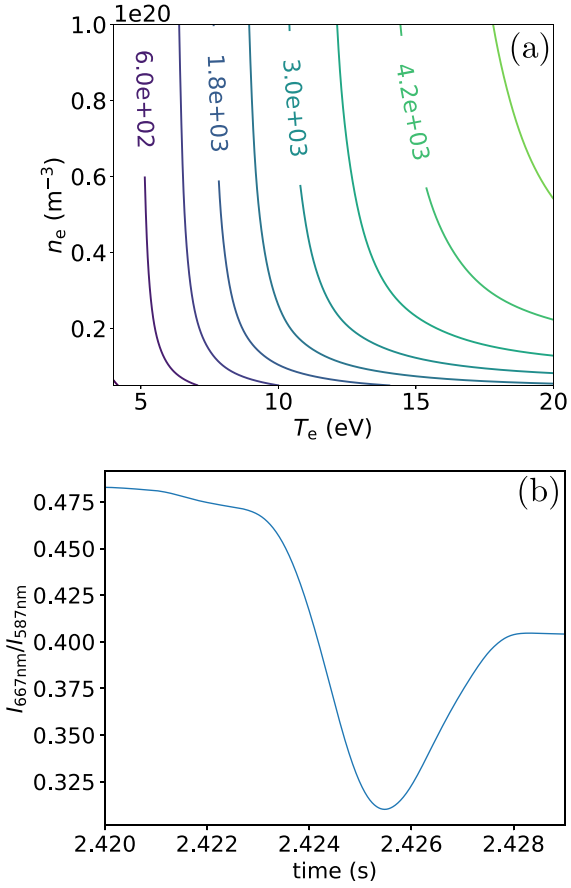

Figure 7. The photon emissivity coefficient of the 587.6 nm helium line multiplied with the electron density in arbitrary units as a function of temperature and density in (a). This diagram was created with the photo emission coefficients of Atomic Data and Analysis Structure [25]. Figure (b) shows the intensity ratio of the helium line 667 nm and 587 nm during an OS to FS transition.

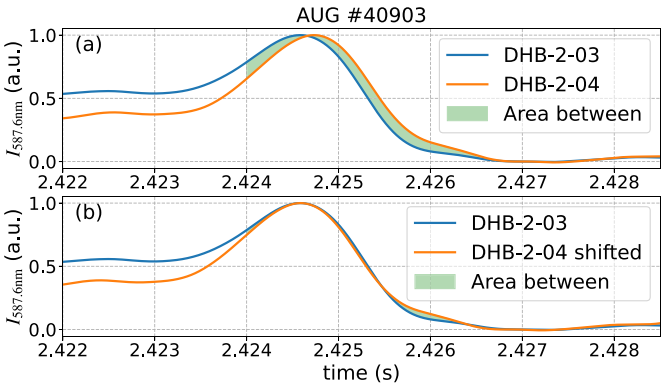

Figure 8. Demonstration of the routine to determine the time shift between neighbouring DHB channels. (a) shows the original, temporally displaced signals, and (b) shows the orange curve shifted by 147 µs in time as a result of minimising the confined area (shaded in green) between the curves. For visualisation, all curves are smoothed with a sliding Hanning window of 1.0 ms and are normalised to their maximal and minimal values.

To prove that this measurement is no artefact due to the neutral helium concentration, this method was also performed to the ratios $I_{667\,nm}/I_{728\,nm}$ and $I_{728\,nm}/I_{706\,nm}$ which are typically used for density and temperature reconstruction. It gives the same order of magnitude for the propagation velocity from $(40 \pm 9)\,m\,s^{-1}$ to $(90 \pm 12)\,m\,s^{-1}$ for the different line ratios and discharges. The absolute results with line ratios should be handled with great care because it was impossible to make a proper background subtraction due to the fast-changing background. The temperature measurements of three target LPs also consistently show a propagation of the temperature collapse from separatrix to far SOL at a propagation velocity between $20\,m\,s^{-1}$ and $50\,m\,s^{-1}$. Both the plots of the ratios and the LP are not shown here.

These measurements give a further indication that the explanations of [12–15] and that of [17] can be correct. The process starts at the separatrix as could be expected in both an $\boldsymbol{E} \times \boldsymbol{B}$-driven bifurcation process and one driven by neutral particles propagating through the PFR. However, no conclusions can be drawn from the measured velocity to the models of [12–15] and [17] as this is the velocity of the temperature collapse which neither model predicts. It should only be noted that the velocity is in the order of magnitude of the radial $\boldsymbol{E} \times \boldsymbol{B}$ drift [18, 27], although this cannot be used to verify the proposed underlying mechanisms [12–15, 17].

To have a deeper look at the detachment process, it is planned to determine the complete 2D profiles of density and temperature with full spatial and temporal resolution. In addition, the electric fields and, thus, the $E \times B$ drift will be reconstructed via the integration of Ohm's law with the electron temperature profiles from the helium beam and the measurement of the LPs. The method is described in [18].

5. Conclusion and outlook

With the DHB diagnostic, it is now possible to analyse 2D electron temperature, density, and pressure profiles with high temporal and spatial resolution. It was used to study the OS to FS transition in the lower outer divertor of ASDEX Upgrade during L-mode discharges. Pressure conservation was confirmed along the magnetic flux surfaces in the divertor. It was also shown that electron temperature and density gradients develop along the flux surfaces during the OS to FS transition. Moreover, the temperature collapse of SSDOs between OS and FS in the outer divertor region was investigated. For the first time, we were able to track the spatial movement of the SSDOs locally. Using two methods, it was found that the temperature collapse of SSDOs starts at the target and propagates with a velocity of $(58 \pm 10)\,m\,s^{-1}$ measured in one poloidal plane along the magnetic flux surfaces to the X-point. It was also possible to measure a perpendicular velocity of $(41 \pm 12)\,m\,s^{-1}$, starting from the separatrix towards the SOL. Since in the models of the SSDOs [12–15] and the model of the detachment cliff [17], the transition is supposed to start at the separatrix, they are consistent in this point. The measured propagation velocity are of the order of the radial $\boldsymbol{E} \times \boldsymbol{B}$ velocity. However, this does not allow any conclusions to be drawn about the underlying physical process.

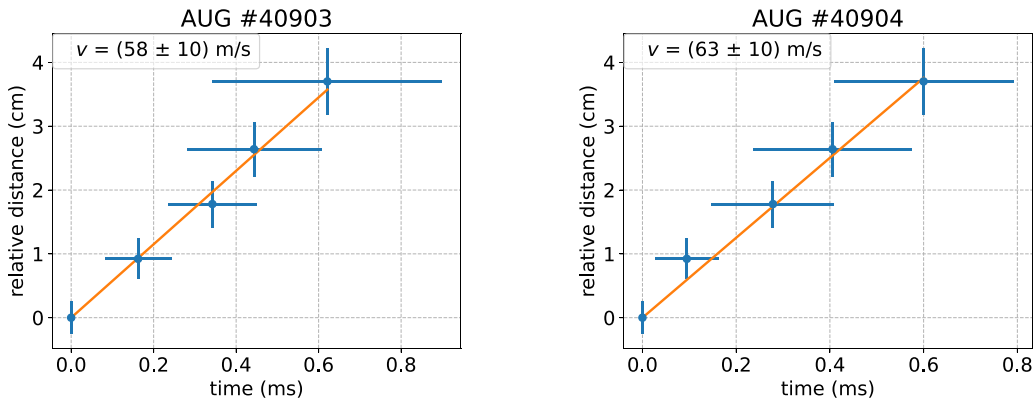

Figure 9. Time shift of the signal for channels located along the same magnetic flux surface plotted against the relative distance between the channels, with discharge #40903 on the left and discharge #40904 on the right side. The data are smoothed by 10 μs. The distance is measured relative to the first channel, which is located at a distance of (3.0 ± 0.3) cm from the target. The velocity calculated via a linear fit is shown in the inlet.

For the upcoming AUG campaign, it is planned to use the constructed electron temperature profiles and the LP measurements to determine the electric fields and thus the $\boldsymbol{E} \times \boldsymbol{B}$ drift in the divertor. The method will be based on integrating Ohm's law as described in detail in [18]. This will help us to investigate the models of detachment cliff and the SSDOs further.

Data availability statement

The data cannot be made publicly available upon publication because they are not available in a format that is sufficiently accessible or reusable by other researchers. The data that support the findings of this study are available upon reasonable request from the authors.

Acknowledgments

This work has been carried out within the framework of the EUROfusion Consortium, funded by the European Union via the Euratom Research and Training Programme (Grant Agreement No 101052200 – EUROfusion). Views and opinions expressed are however those of the author(s) only and do not necessarily reflect those of the European Union or the European Commission. Neither the European Union nor the European Commission can be held responsible for them.

Author contributions

S Hörmann 0009-0004-5704-7114
Data curation (equal), Formal analysis (lead), Investigation (lead), Methodology (lead), Project administration (supporting), Software (lead), Validation (lead), Visualization (lead), Writing – original draft (lead), Writing – review & editing (equal)

M Cavedon 0000-0002-0013-9753
Conceptualization (lead), Data curation (equal), Formal analysis (supporting), Funding acquisition (supporting), Investigation (supporting), Methodology (supporting), Project administration (lead), Resources (supporting), Software (supporting), Supervision (equal), Validation (supporting), Writing – review & editing (equal)

M Griener 0000-0003-2953-536X
Conceptualization (supporting), Data curation (equal), Formal analysis (supporting), Funding acquisition (supporting), Investigation (supporting), Methodology (supporting), Project administration (supporting), Resources (supporting), Software (supporting), Supervision (equal), Validation (supporting), Writing – review & editing (equal)

D Wendler 0000-0002-8838-0137
Data curation (supporting), Formal analysis (supporting), Project administration (supporting), Software (supporting)

D Brida 0000-0002-8647-7058
Formal analysis (supporting), Investigation (supporting), Methodology (supporting)

E Wolfrum 0000-0002-6645-6882
Formal analysis (supporting), Investigation (supporting), Methodology (supporting), Writing – review & editing (equal)

U Stroth 0000-0003-1104-2233
Funding acquisition (lead), Investigation (supporting), Methodology (supporting), Writing – review & editing (equal)

References

[1] Pitts R *et al* 2019 Physics basis for the first ITER tungsten divertor *Nucl. Mater. Energy* **20** 100696
[2] Federici G, Biel W, Gilbert M, Kemp R, Taylor N and Wenninger R 2017 European DEMO design strategy and consequences for materials *Nucl. Fusion* **57** 092002
[3] Pitts R *et al* 2017 Physics conclusions in support of ITER W divertor monoblock shaping *Nucl. Mater. Energy* **12** 60–74
[4] Escourbiac F, Durocher A, Fedosov A, Hirai T, Pitts R, Gavila P, Riccardi B, Kuznetcov V, Volodin A and

Komarov A 2019 Assessment of critical heat flux margins on tungsten monoblocks of the ITER divertor vertical targets *Fusion Eng. Des.* **146** 2036–9
[5] Loarte A *et al* 1998 Plasma detachment in JET Mark I divertor experiments *Nucl. Fusion* **38** 331
[6] Lipschultz B *et al* 1995 Dissipative divertor operation in the alcator C-Mod tokamak *J. Nucl. Mater.* **220–222** 50–61
[7] Petrie T *et al* 1997 Radiative divertor experiments in DIII-D with D_2 injection *Nucl. Fusion* **37** 321
[8] Kallenbach A *et al* the ASDEX Upgrade Team 2015 Partial detachment of high power discharges in ASDEX Upgrade *Nucl. Fusion* **55** 053026
[9] Potzel S, Wischmeier M, Bernert M, Dux R, Müller H and and A S 2013 A new experimental classification of divertor detachment in ASDEX upgrade *Nucl. Fusion* **54** 013001
[10] Potzel S, Wischmeier M, Bernert M, Dux R, Müller H and Scarabosio A 2013 Characterization of the fluctuating detachment state in ASDEX Upgrade *J. Nucl. Mater.* **438** S285–90
[11] Scotti L, Cavedon M, Bernert M, Brida D, Kurzan B, Dux R and the ASDEX Upgrade Team 2024 Existence of a detachment cliff at ASDEX upgrade *Plasma Phys. Control. Fusion* **66** 075004
[12] Heinrich P *et al* (ASDEX Upgrade team) 2020 Self-sustained divertor oscillations in ASDEX Upgrade *Nucl. Fusion* **60** 076013
[13] Krasheninnikov S, Kukushkin A, Pistunovich V and Pozharov V 1987 Self-sustained oscillations in the divertor plasma *Nucl. Fusion* **27** 1805
[14] Kukushkin A S and Krasheninnikov S I 2019 Bifurcations and oscillations in divertor plasma *Plasma Phys. Control. Fusion* **61** 074001
[15] Krasheninnikov S I, Kukushkin A S and Pshenov A A 2016 Divertor plasma detachment *Phys. Plasmas* **23** 055602
[16] McLean A *et al* 2015 Electron pressure balance in the sol through the transition to detachment *J. Nucl. Mater.* **463** 533–6
[17] Jaervinen A E *et al* 2018 $E \times B$ flux driven detachment bifurcation in the DIII-D tokamak *Phys. Rev. Lett.* **121** 075001
[18] Stangeby P, Elder J, McLean A and Watkins J 2017 Experimentally-based $E \times B$ drifts in the DIII-D divertor and SOL calculated from integration of ohm's law using thomson scattering measurements of T_e and n_e *Nucl. Mater. Energy* **12** 876–81
[19] Du H, Zheng G, Guo H, Jaervinen A E, Duan X, Bonnin X, Eldon D and Wang D 2020 SOLPS analysis of the necessary conditions for detachment cliff *Nucl. Fusion* **60** 046028
[20] Hörmann S *et al* 2024 Thermal helium beam diagnostic for 2D profile measurements in the divertor of ASDEX Upgrade *Rev. Sci. Instrum.* **95** 113507
[21] Rognlien T *et al* 2017 Comparison of 2D simulations of detached divertor plasmas with divertor Thomson measurements in the DIII-D tokamak *Nucl. Mater. Energy* **12** 44–50
[22] Cavedon M *et al* (the ASDEX Upgrade Team) 2022 Experimental investigation of L- and H-mode detachment via the divertor Thomson scattering at ASDEX Upgrade *Nucl. Fusion* **62** 066027
[23] Griener M, Wolfrum E, Cavedon M, Dux R, Rohde V, Sochor M, Muñoz Burgos J M, Schmitz O and Stroth U 2018 Helium line ratio spectroscopy for high spatiotemporal resolution plasma edge profile measurements at ASDEX Upgrade (invited) *Rev. Sci. Instrum.* **89** 10D102
[24] Griener M *et al* (ASDEX Upgrade Team) 2017 Fast piezoelectric valve offering controlled gas injection in magnetically confined fusion plasmas for diagnostic and fuelling purposes *Rev. Sci. Instrum.* **88** 033509
[25] Summers H P 2004 Atomic data and analysis structure user manual, version 2.7 ed. *Atomic Data and Analysis Structure* (available at: www.adas.ac.uk)
[26] Rodriguez-Gonzalez A, Cruz-Zabala D J, McKay K, Griener M, Plank U, Viezzer E, Rohde V and Dux R (ASDEX Upgrade Team) 2025 Understanding and modeling of gas puff injection for diagnostic purposes *Rev. Sci. Instrum.* **96** 013506
[27] Wu H, Subba F, Wischmeier M, Cavedon M and Zanino R (the ASDEX Upgrade Team) 2021 SOLPS-ITER modeling of ASDEX Upgrade L-mode detachment states *Plasma Phys. Control. Fusion* **63** 105005